Papers in Natural Resources   Natural Resources, School of

2017

Carbon Flux Phenology from the Sky: Evaluation for Maize and Soybean

Alexandria G. McCombs
University of South Carolina, Columbia, amccombs@email.sc.edu

Cuizhen Wang
University of South Carolina, Columbia

Ankur Desai
University of Wisconsin–Madison

Andrew E. Suyker
University of Nebraska - Lincoln, asuyker@unl.edu

Sebastien C. Bird
Lawrence Berkley National Laboratory, Berkeley

Carbon Flux Phenology from the Sky: Evaluation for Maize and Soybean

ALEXANDRIA G. MCCOMBS, APRIL L. HISCOX, AND CUIZHEN WANG

Department of Geography, University of South Carolina, Columbia, South Carolina

ANKUR R. DESAI

Department of Atmospheric and Oceanic Sciences, University of Wisconsin–Madison, Madison, Wisconsin

ANDREW E. SUYKER

School of Natural Resources, University of Nebraska–Lincoln, Lincoln, Nebraska

SEBASTIEN C. BIRAUD

Climate Sciences Department, Lawrence Berkley National Laboratory, Berkeley, California

ABSTRACT

Carbon flux phenology is widely used to understand carbon flux dynamics and surface exchange processes. Vegetation phenology has been widely evaluated by remote sensors; however, very few studies have evaluated the use of vegetation phenology for identifying carbon flux phenology. Currently available techniques to derive net ecosystem exchange (NEE) from a satellite image use a single generic modeling subgroup for agricultural crops. But, carbon flux phenological processes vary highly with crop types and land management practices; this paper reexamines this assumption. Presented here are an evaluation of ground-truth remotely sensed vegetation indices with in situ NEE measurements and an identification of vegetation indices for estimating carbon flux phenology metrics by crop type. Results show that the performance of different vegetation indices as an indicator of phenology varies with crop type, particularly when identifying the start of a season and the peak of a season. Maize fields require vegetation indices that make use of the near-infrared and red reflectance bands, while soybean fields require those making use of the shortwave infrared (IR) and near-IR bands. In summary, the study identifies how to best utilize remote sensing technology as a crop-specific measurement tool.

1. Introduction

Phenological dynamics are key to identifying changes in growing season and how they change with global climate change (Zhang et al. 2003). Many human-managed landscapes have been shown to have a significant impact on carbon flux dynamics between terrestrial ecosystems and the atmosphere, and therefore they are a major factor in climate change. The responses of the global carbon cycle as a result of human-managed landscapes are a significant source of uncertainty in future climate projections (Le Quéré et al. 2015). Phenology metrics have been derived for identifying changes in vegetation type and length of growing season as a result of climate change. The vegetation phenology in agricultural systems has posed great challenges in modeling of carbon dynamics because of human interference, and therefore it will not always follow the same time-resolved signatures as other landscapes, for instance, forests within the same climatic zone may have varying phenology because of human management practices (Walker et al. 2012).

Carbon flux phenology (CFP) metrics is a method that has been used for tracking changes in carbon dynamics within an ecosystem, and it can be directly derived from field-based measurements such as net ecosystem exchange (NEE) and PhenoCams (e.g., Noormets et al. 2009; Klosterman et al. 2014). The physiological stages of crops are highly correlated to CFP, where CFP identifies five recurring transition periods that occur

Corresponding author: Alexandria G. McCombs, amccombs@email.sc.edu

annually in NEE measurements (Garrity et al. 2011; Viña et al. 2011; Balzarolo et al. 2016). Wu et al. (2012) demonstrated the importance of identifying the true length of the carbon uptake period by showing the strong correlation between the carbon uptake period and net ecosystem production (NEP). When the carbon uptake period is delayed by one day, there can be a reduction in NEP estimates of 16.1 gC m^{-2} in nonforested land covers (Wu et al. 2012). Limited ground-based carbon flux observations make it difficult to scale the total contribution of agricultural land management to the carbon budget. Unfortunately, ground-based measurements represent finer spatial scales (typically <10 km^2) and show significant changes occurring on time scales as short as 30 min. Meanwhile, PhenoCams cover a single field, but they do not represent a landscape for the region. Therefore, to represent a broader area, satellite remote sensing has been used for estimating regional phenology dynamics (Wang et al. 2011).

Work by Wang et al. (2011) made use of satellite remote sensing for differentiating between grass types (i.e., C$_3$ or C$_4$ grasses) and row crops. Their work uses the 500-m 8-day MODIS normalized difference vegetation index (NDVI) time series to examine the crop and grassland phenology and gives several statistics that can successfully delineate a variety of grass types as well as major row crops. Wang et al. (2011) showed there are differences in the phenological signals of different crop types and grass types.

Previous work that has sought to identify CFP metrics and carbon dynamics in agricultural landscapes have often used a single vegetation index (VI) calculated from remote sensing imagery to model for all crop types. This is a limitation of many remote sensing models because agricultural lands are grouped into a single land-cover category, ignoring the variations in physiology of different crop types and management practices (e.g., Fu et al. 2014; Dong et al. 2015; Xiao et al. 2011; and others). This is known to be inaccurate, as field-based studies have found that the gas exchange between different crop types and land management procedures are not uniform (e.g., Gebremedhin et al. 2012; Frank and Dugas 2001; Cicuéndez et al. 2015; and others). This makes the regional prediction of ecosystem–atmosphere energy and gas exchange particularly challenging in agricultural lands.

The two most accessible datasets for estimating phenology are MODIS and Landsat, but they do not provide comparable spatial and temporal coverage. The daily and weekly 500-m spatial resolution of MODIS is too coarse over a heterogeneous landscape to accurately represent agricultural flux environments, while the 16-day return period of the finer spatial resolution

Landsat is spaced too far in time to capture the daily changes that can occur in agricultural environments. Zhu et al. (2010) developed methods to address this by fusing the datasets to create a time series of Landsat and MODIS using the Enhanced Spatial and Temporal Adaptive Reflectance Fusion Model (daily) (ESTARFM). This methodology can be used to maintain the temporal resolution of MODIS and the spatial resolution of Landsat (30-m pixels) to create "Landsat like" MODIS images, a spatial time series of VIs for aiding in the identification of CFP metrics, and discrimination of vegetation type (Wang et al. 2011; Price et al. 2002; Guo et al. 2003).

Here, we will identify the best VI for identifying satellite remote sensing–derived phenology metrics to estimate crop-based CFP metrics to improve models of energy and gas exchange. Multiple methods exist to remotely estimate CFP, but they have rarely been compared. The work presented here evaluates which VIs best identify CFP metrics derived from downscaled MODIS and Landsat satellite observations. This was done by comparing ground-observed CFP transition periods from eddy covariance flux tower observations of NEE to satellite-derived phenology metrics. We present here an evaluation of the effectiveness of 10 VIs in maize (C$_4$ photosynthetic pathway) and soybean (C$_3$ photosynthetic pathway) agricultural fields, and a method for comparison of these spatially disparate measures. We hypothesize that the most effective remotely sensed VIs for determining CFP metrics will vary based on crop types as a result of the variation in biomass that can be observed in the field of view, and the differences in plant physiology between maize and soybean.

2. Datasets and preprocessing

a. Remote sensing datasets

During the study period from 2002 to 2011, numerous satellite observations have been archived for the U.S. Great Plains region. Here, we utilized land surface reflectance datasets from MODIS (500-m resolution) and Landsat (30-m resolution). The 8-day 500-m MODIS surface reflectance product (MOD09A1) was obtained for 2002–11 for the three tiles that covered the five AmeriFlux sites of interest (Vermote 2015; Wan et al. 2015). The data were downloaded from the Land Processes Distributed Active Archive Center (LP DAAC) managed by NASA.

The MOD09A1 data product provides the spectral surface reflectance using MODIS bands 1–7. Each pixel contains the highest-quality higher-order gridded level-2 (L2G) observation over an 8-day period (Fig. 1, steps 2 and 3). The use of this dataset minimizes the
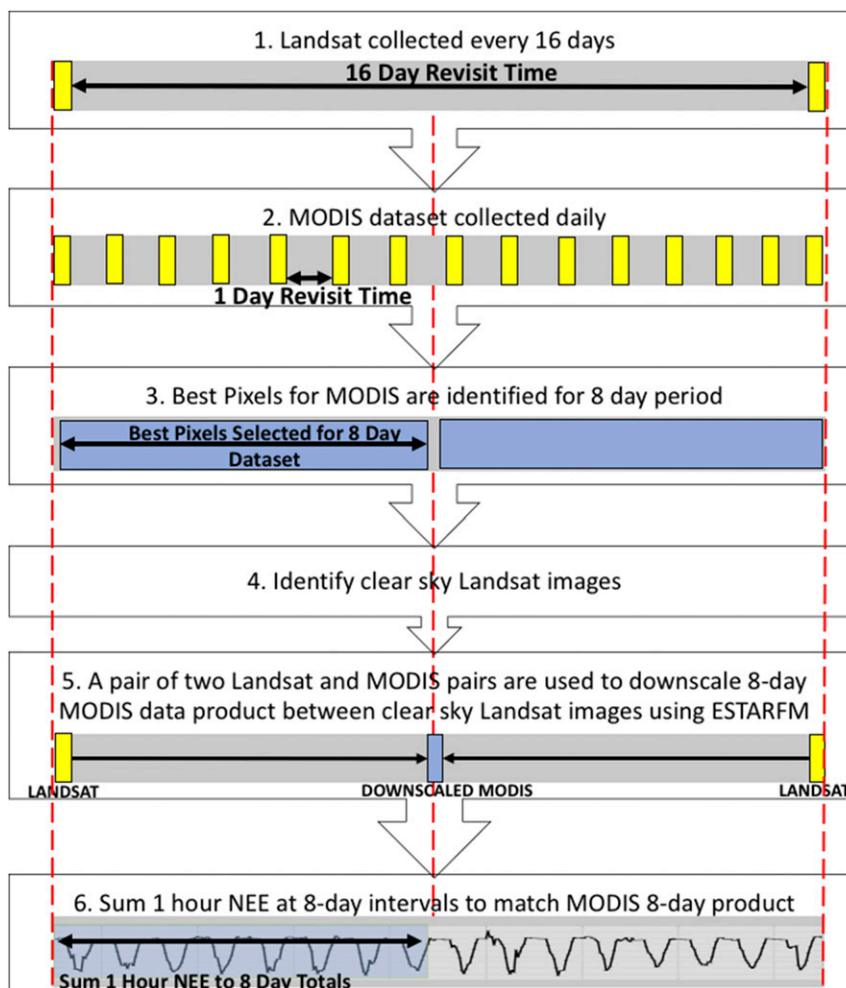
FIG. 1. Illustration of the process for scaling all data to the same temporal resolution. Data products after georectification and atmospheric correction but no other data manipulation has occurred (yellow boxes). Data that has been manipulated in some way, which would include the downscaling algorithm or summing datasets (blue boxes). In step 1 Landsat reflectance data represent a 16-day revisit time. In step 2 MODIS datasets are collected at a daily time scale and each unprocessed image is represented (yellow box). In step 3 NASA selects the best pixels from the previous 8 days to represent the entire 8-day period. In step 4, clear-sky pairs of Landsat and MODIS imagery were manually identified. Step 5 shows how the Landsat, which occurs before the 8-day period or after the 8-day period, but not during the 8-day period, is used to downscale the MODIS observations to have a 30-m spatial resolution using ESTARFM to create an 8-day time series of Landsat–MODIS fused imagery. Last, step 6 represents the hourly NEE values that are summed to an 8-day total that matches the satellite remote sensing product time stamp. Further comparisons discussed in the text are made between the summed NEE (blue box in step 6) and the final fused image (blue box in step 5).

influences of clouds that will occur in the daily MODIS files. The state flags provided with the dataset were applied to each image to mask cloudy pixels, snow or ice, and cloud-shadowed pixels. Each image was subset to a 10 km × 10 km area around the station to ensure the entirety of the station fetch was included within the subset image (Horst and Weil 1994; Leclerc and Foken 2014, 213–214) and to reduce processing time.

Landsat datasets have a 16-day revisit cycle and 30-m spatial resolution (Fig. 1, step 1). Images from the *Landsat-5* Thematic Mapper and the *Landsat-7* Enhanced Thematic Mapper Plus were used. All Landsat data were acquired from the U.S. Geological Survey's (USGS) Earth Resources Observation and Science Center Science Processing Architecture. This product has been atmospherically corrected and geometrically corrected

TABLE 1. AmeriFlux/FluxNet stations for NEE-based carbon flux phenology metrics. Oklahoma (OK). Nebraska (NE). Minnesota (MN).

Station ID	Station name	Crop type	Soil type	Annual mean air temperature (°C)	Annual mean precipitation (mm)	Data availability
US-ARM[a]	OK—ARM Southern Great Plains site	Maize–soybean–wheat rotation	Kirkland loams[a]	14.5[b]	902[b]	2003–11
US-Ne1[c]	NE—Mead irrigated	Maize	Yutan silt[c]	10.1[b]	854[b]	2002–11
US-Ne2[c]	NE—Mead irrigated rotation	Maize–soybean rotation	Yutan silt[c]	10.1[b]	854[b]	2002–11
US-Ne3[c]	NE—Mead rain fed	Maize–soybean rotation	Yutan silt[c]	10.1[b]	854[b]	2002–11
US-Ro1[d]	MN—Rosemount G21 conventional management corn soybean rotation	Maize–soybean rotation	Kennebec silt loam	6.9[b]	888[b]	2004–11

[a] Raz-Yaseef et al. (2015).
[b] Vose et al. (2014).
[c] Verma et al. (2005).
[d] Griffis et al. (2011).

using the same subroutines conducted on MODIS surface reflectance datasets, making these two datasets comparable (Masek et al. 2006). The files downloaded contained surface reflectance, cloud mask, and quality assurance flags. The blue (450–520 nm), green (520–600 nm), red (630–690 nm) near-infrared (NIR, 760–900 nm), and two shortwave-infrared surface reflectance bands (SWIR1, 1550–1750 nm; SWIR2, 2080–2350 nm) were used in this analysis. The 10 km × 10 km subsets of all Landsat surface reflectance products were created to match the subset of the MODIS datasets. Using the quality control and cloud flags provided by USGS, all pixels labeled as cloud, adjacent to cloud, snow/ice, or poor quality were removed.

b. ESTARFM downscaling model

The subset images were processed in the ESTARFM image fusion algorithm (Zhu et al. 2010). The MODIS bands 1–7 were reordered to spectrally match those bands found in Landsat imagery. For instance, MODIS band 1 (red band) became band 3 to have the same band placement as the red band in the Landsat file. The MODIS surface reflectance was then spatially resampled from a spatial resolution of 500 to 30 m to match Landsat using standard raster resampling methodology described in DeMers (2002). The image fusion resulted in up to 46 time stamps annually, which made use of the benefits of the finer spatial resolution and higher temporal resolution of both satellites (Wang et al. 2013; Walker et al. 2012).

To downscale a MODIS image to a 30-m pixel size, ESTARFM requires two Landsat–MODIS imagery pairs that occur within the same 8-day period to run: one pair of images occurs before the MODIS image to be downscaled and one pair of images that occurs after (Fig. 1, step 4–5). All Landsat–MODIS imagery pairs were identified using the cloud mask dataset from MODIS and Landsat: if both temporally matching MODIS and Landsat subset images had ≤10% clouds, then the pair was used for downscaling. This was done because the image pairs need to be as cloud and snow/ice free as possible for the ESTARFM algorithm to work. Figure 1 illustrates this process in steps 2–4. More information about how the algorithm downscales the 500-m MODIS to 30-m spatial resolution can be found in Gao et al. (2006) and Zhu et al. (2010). The ESTARFM methodology creates a spatial time series of Landsat-like surface reflectance, which is a downscaled MODIS image to 30-m Landsat spatial resolution, and includes the blue, green, red, NIR, SWIR1, and SWIR2 bands. The Landsat-like surface reflectance time series are later used to calculate VIs for aiding in the identification of CFP metrics (Wang et al. 2011; Price et al. 2002; Guo et al. 2003; Fang et al. 2013; Garrity et al. 2011)

c. Net ecosystem exchange

Tower-based carbon flux observations are used as the ground-truth control data points for VIs discussed below. These observations come from FluxNet, a confederation of regional networks of flux towers (Running et al. 1999; Papale et al. 2015; Baldocchi et al. 2001). One data provider to FluxNet is AmeriFlux, which is a network of Primary Investigator (PI)-managed sites measuring carbon, water, and energy fluxes within the Americas. These sites include the most continuous and reliable observations of carbon flux data available in the United States. We focus here on five sites located in the U.S. Great Plains with multiyear data availability from 2002 to 2011. The five stations selected are located on fields growing either maize, maize/soybean rotation, or maize/soybean/wheat rotation. There were 15 site years for soybean and 27 site years for maize. Table 1 provides a summary of the stations and their data availability.

Since CFP is a direct function of net carbon exchange, NEE was the primary variable used in this analysis. The goal of this analysis was to compare remotely sensed phenology metrics to NEE phenology metrics from tower-based observations. NEE is directly measured using the eddy covariance technique and averaged at 30- or 60-min intervals. The eddy covariance system makes use of a 3D sonic anemometer as well as an open- or closed-path CO_2 and H_2O gas analyzer that is collocated with the sonic anemometer. Since each station is individually managed, the specific instrumentation (manufacturer, model, etc.) varies. However, all data are collected and quality controlled by following best practices for flux observations (Baldocchi et al. 2001).

To use NEE as a basis for comparison, a time series matching the remote sensing data was constructed. To do this, it was desirable to find a total NEE value occurring at the times coincident with remote sensing products. The tier 1 FLUXNET2015 dataset was used. All FLUXNET2015 datasets have gone through extensive quality control measures and gap filling has been conducted on the datasets. All gap-filled datasets use the gap-filling method described in Vuichard and Papale (2015). One exception to the processing method was the Rosemount G21 Conventional Management Corn Soybean Rotation station (US-Ro1) located in Minnesota (Griffis et al. 2011). For this site the FLUXNET2015 dataset was not available. The gap-filled level 2 AmeriFlux dataset was used instead. All level 2 gap-filled datasets are gap-filled data by individual PIs and may not use the same methodology as the FLUXNET2015 dataset.

Gap-filled NEE values were converted from hourly or half-hourly NEE values in $[\mu\text{molCO}_2\,\text{m}^{-2}\,\text{s}^{-1}]$ to $[\text{gC}\,\text{m}^{-2}\,\text{h}^{-1}]$ and then summed for the 8-day period that was coincident to the time stamp of the remote sensing images. This provides NEE values in units of $[\text{gC}\,\text{m}^{-2}\,8\,\text{days}^{-1}]$. The process of matching NEE measurements to the remote sensing data is shown in Fig. 1. Steps 1–5 are the ESTARFM technique discussed below, and step 6 shows the computation of an 8-day NEE value.

One concern when working with carbon flux measurements is whether the NEE values represent the land cover that is being evaluated. To determine whether the predominant source locations of NEE fell within the represented agricultural field, a surface-layer footprint climatology analysis was conducted on all the sites (Fig. 2). The footprint climatology was computed using the model developed by Kljun et al. (2015) for non-gap-filled observations. All footprint climatologies had a 90% source contribution that fell within the agricultural field represented by the flux tower. This provides an independent confirmation that NEE values represent the agricultural crop. Therefore, data were not scaled

to a flux footprint because the samples represent the crop field a majority of the time. During stable boundary layer conditions, source locations may fall outside the agricultural field. However, because the temporal resolution of the data had been reduced from 30-min observations to 8-day totals, the nighttime respiration made up a small fraction of the total NEE value and was therefore not omitted from the 8-day total NEE.

3. Methods

a. Vegetation indices

The Landsat-like time series were used to determine a number of crop-related VIs. The most familiar of these are NDVI (Rouse et al. 1974) and the enhanced vegetation index (EVI) (Huete et al. 1997, 2002), but we extend our analysis to eight additional indices that have been used throughout the literature for their sensitivity in agricultural regions. Each of the VIs was selected for the specific information it provides about the land surface. Table 2 provides a summary of all the VIs evaluated. The temperature and humidity of the stations were not considered for this analysis because vegetation indices have been shown to be a function of temperature, precipitation, and NEE (Bonan 2008; Wu et al. 2017; Frank and Karn 2003).

b. Extraction of field-scale measurements

Crop types grown in each agricultural field where the AmeriFlux site was located was provided by the station PI. To obtain statistics on surface attributes for the representative agricultural field, a polygon shapefile was created to extract pixel values for each downscaled Landsat-like VI value for all years from 2002 to 2011. The mean and standard deviation of the extracted values from each image were computed to create an 8-day time series of the 10 VIs at field scale. If any pixel value was previously removed because of poor quality, or the value fell outside the upper and lower bounds of the VI, it was also removed from the computation of the field-scale statistics.

c. Comparison of VI-based and NEE-based phenology metrics

The CFP variables of interest include start of season (SOS), sink (SINK), peak of season (POS), source (SOURCE), and end of season (EOS) from both the NEE measurements and the VIs. From this point forward, subscripts NEE and VI will be used to denote which data source was used to find the phenological metric. All NEE-based metrics were estimated using the ground-based direct measurement of carbon dynamics between the atmosphere and the ecosystem. The VI-based metrics were
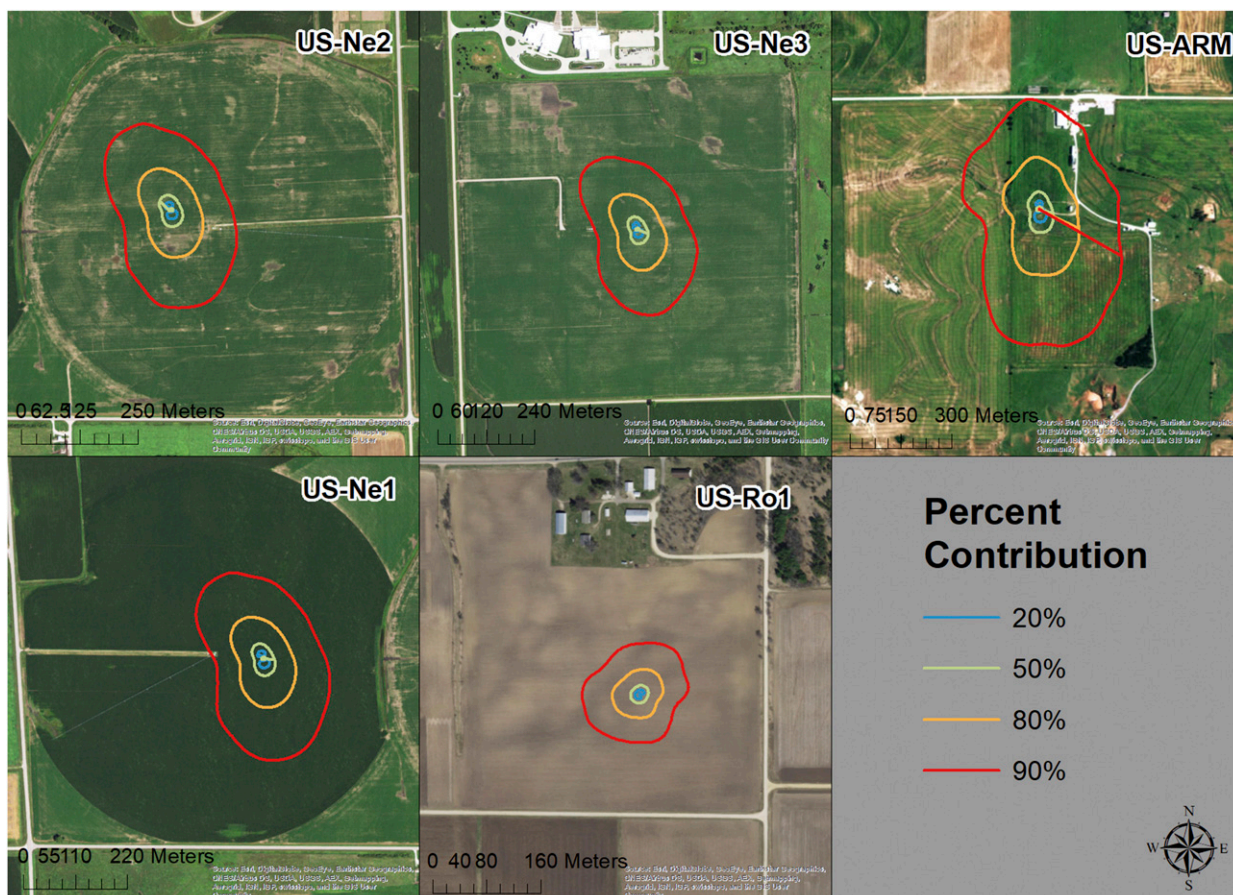
FIG. 2. Daytime footprint climatology for (upper left) US-Ne2, (upper middle) US-Ne3, US-ARM (upper right), (lower left) US-Ne1, and (lower middle) US-Ro1 for 2005 using the Kljun et al. (2015) footprint model. Climatology indicates that 90% (red line) of the footprint falls within the represented agricultural field.

estimated using VIs that were calculated from satellite remote sensing and were assessed in this study against the NEE-based metrics. The units for each phenological metric are day of the year (DOY) when it occurs.

All NEE and VI data were divided by year and station based on the crop type grown each site year. There were 27 site years of maize and 15 site years of soybean.

Soybean and maize were the main focus of this analysis; therefore, the years that the US-ARM station grew wheat or canola were not included (Raz-Yaseef et al. 2015). Specific land management activities of the agricultural fields were not considered.

Using the tower measurements, $SINK_{NEE}$, $SOURCE_{NEE}$, SOS_{NEE}, EOS_{NEE}, and POS_{NEE} metrics were determined

TABLE 2. Vegetation indices evaluated for determining the SOS, EOS, SINK, SOURCE, and POS in carbon flux phenology.

| Vegetation index	Equation
NDVI (Rouse et al. 1974)	(NIR − RED) / (NIR + RED)
EVI (Huete 1997, 2002)	2.5 [(NIR − RED) / (NIR + 6*RED − 7.5*BLUE + 1)]
NDTI (Shen and Tanner 1990)	(SWIR1 − SWIR2) / (SWIR1 + SWIR2)
NDSVI (Qi et al. 2002)	(SWIR1 − RED) / (SWIR1 + RED)
STI (van Deventeer et al. 1997)	SWIR1/SWIR2
SAVI (Huete 1988; Huete et al. 1994)	[(NIR − RED)/(NIR + RED + L)][1 + L], L = 0.5
GNDVI (Gitelson and Merzlyak 1998)	(NIR − GREEN)/(NIR + GREEN)
NDI7 (McNairn and Protz 1993)	(NIR − SWIR2)/(NIR + SWIR2)
Moisture stress index (Rock et al. 1986)	SWIR1/NIR
LSWI (Xiao et al. 2005, 2004)	(NIR − SWIR2)/(NIR + SWIR2)
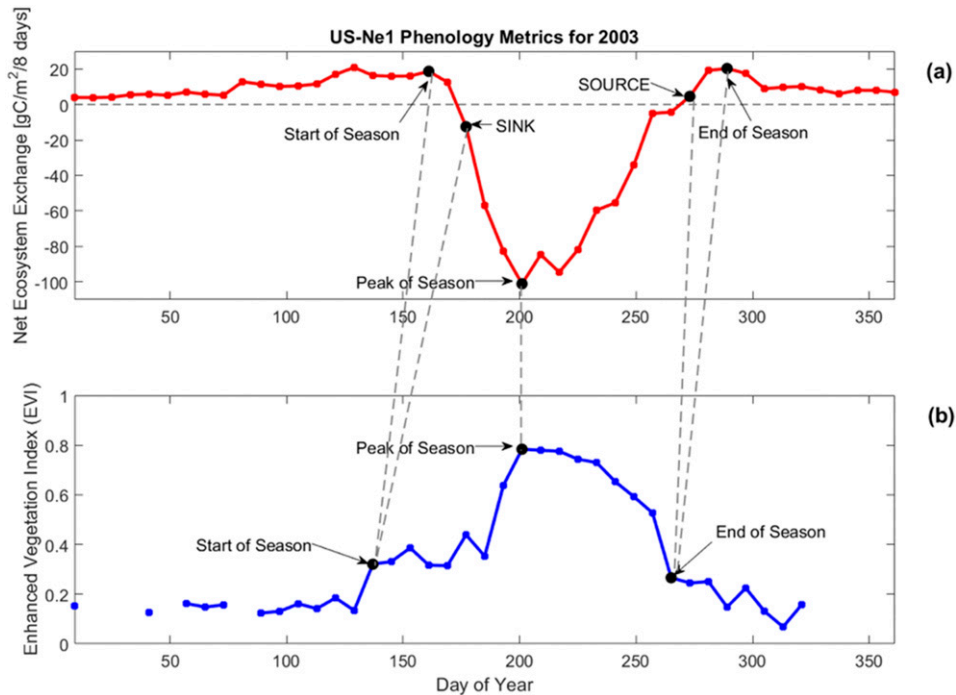
FIG. 3. Time series of (a) NEE and (b) EVI for 2003 at the US-Ne1 station. NEE (red dots) and EVI (blue dots) 8-day values. Transition points for VI-based and NEE-based phenology metrics (black dots). Illustration of how the phenology metrics were compared (gray dashed lines). In (a) start of season is the point where photosynthetic acclimation begins, carbon sink (SINK) is the point in time when NEE becomes negative, peak of season is the peak carbon uptake, carbon source (SOURCE) is the point in time when NEE becomes positive again, and end of season is the date when photosynthesis ceases. Values will not necessary fall on a value of zero for SINK and SOURCE, so the first value after the zero line is crossed was selected. In (b) start of season is the point when EVI is greater than 20% of the total amplitude for the year, peak of season is the peak greenness, and end of season is the day when EVI is less than 20% of the total amplitude for the year.

using the methodology defined in Garrity et al. (2011). SOS_{NEE} was determined as the time stamp following the peak of ecosystem respiration in the spring, and EOS_{NEE} was determined as the peak of ecosystem respiration in the fall. $SINK_{NEE}$ was the day of year in the spring that NEE became negative, and $SOURCE_{NEE}$ was the day of year in the fall that NEE became positive again. Figure 3a shows the points where these metrics would occur on an annual time series of NEE.

Using the methods discussed in Wang et al. (2011), SOS_{VI} was calculated for the VIs by determining the day of year when the VI increased by 20% of the total amplitude for the entire season. POS_{VI} was the day of year when the maximum VI occurred, and EOS_{VI} was the day of year when the VI decreased to values less than 20% of the total amplitude for the season. These points are shown in Fig. 3b.

The VI-based phenological metrics were compared on a scatterplot to the NEE-based metrics for each crop type. An example of the comparison for EVI is shown in Fig. 4. SOS_{VI} and EOS_{VI} were compared to SOS_{NEE}

and EOS_{NEE}, respectively, to determine whether SOS_{VI} and EOS_{VI} better represented the onset and ceasing of photosynthetic acclimation (SOS_{NEE}, EOS_{NEE}). SOS_{VI} and EOS_{VI} were also compared to $SINK_{NEE}$ and $SOURCE_{NEE}$ to determine how well they represent the day of year when $SINK_{NEE}$ or $SOURCE_{NEE}$ occurs. The phenological metrics are compared against a 1:1 line (gray dashed line, Fig. 4). The mean signed difference (MSD) in days was determined for each phenology point as

$$MSD = \left[\sum (DOY_{NEE,i} - DOY_{VI,i}) \right] \Big/ n, \qquad (1)$$

where i is the corresponding value for the same year and station, and n is the number of values being averaged. The metrics were compared across varying climate conditions, however, temperature and humidity were not considered (Garrity et al. 2011; Peng et al. 2017).

The significance of each of the VIs was tested by calculating the t test using a 10% confidence interval. A VI was considered significant when t was greater than 1.3, as
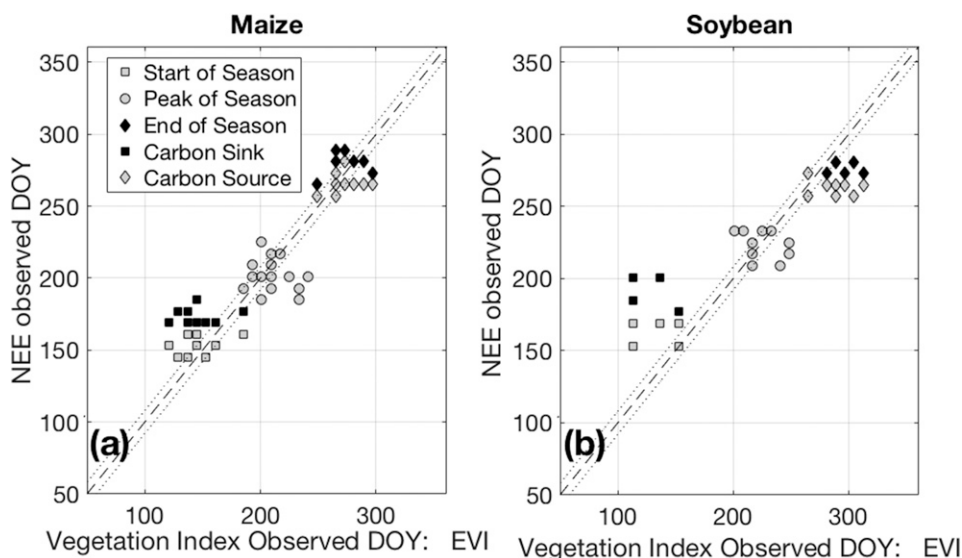
FIG. 4. Scatterplot of carbon flux phenology metrics as determined by the EVI-based data (x axis) and the NEE-based data (y axis) for (a) maize and (b) soybeans. Shown are the 1:1 line (black dashed line) and the ± 8-day bounds (dotted lines).

determined by the degrees of freedom. It was assumed that the population mean was zero during the calculation of the t statistic.

The total NEE value was calculated annually for the growing season by summing NEE from the NEE-based SINK to SOURCE dates. This total carbon uptake value was then compared to the sum of NEE from SOS and EOS dates as estimated by VI-based phenology. The total growing season carbon uptake as estimated from VI-based SOS to EOS for each vegetation index was compared to the total carbon uptake value from NEE-based SINK to SOURCE.

4. Results

When considering the performance of each VI as presented here, it is important to understand that any MSD values less than 8 days is considered to be a good measure because the images used to compute the VI can fall anywhere in the 8-day time stamp of MODIS (Fig. 1, step 5).

In Fig. 4, the scatterplot shows that in general for maize (Fig. 4a) the VI-based versus NEE-based phenological metrics were clustered near the 1:1 line for EVI, where for several site years the VI-based metrics fall before and after the NEE-based metrics. There is a different pattern that occurs in soybean (Fig. 4b) for the same VI, where VI-based SOS were estimated before NEE-based SOS and SINK phenology metrics, and VI-based EOS was estimated after NEE-based SOURCE and EOS dates. A scatterplot for each VI was visually

inspected to visualize the closeness of the VI-based phenology metrics to the NEE-based phenology metrics. These results are included in the text of the following sections. A table of the relevant values for all VIs and phenology points is included in Table 3. It should be noted that several stations had multiple crop rotations in the same year. These stations resulted in erroneously early or late phenology metrics and were therefore emitted from the analysis.

a. Start of season and SINK

In maize fields the VI that best captured SOS_{NEE}, in terms of both absolute difference and variability, was the EVI with an MSD of 4.27 days, a standard deviation of 14.14 days, and a significant t statistic value. This means that, on average EVI estimated the SOS in maize fields 4 days before the true start of season. EVI was able to estimate SOS most consistently from VI-based phenology metrics with a low standard deviation and an absolute difference less than 8 days, which is the number of days between time stamps. Another index that performed well and had significant t statistic values with predictions within 11 days included the soil-adjusted vegetation index (SAVI). The simple tillage index (STI) also had low standard deviation of 9.66 days and a significant t value. Thus, although STI estimated the SOS 30 days after the true SOS, it was consistent in this bias.

In soybean fields, the normalized difference senescent vegetation index (NDSVI) could estimate SOS with a lower standard deviation (12.22 days), a larger MSD

TABLE 3. Average mean signed difference in days between NEE-based phenology metrics and VI-based phenology metrics across all maize, soybean fields, and soybean and maize combined. Positive value indicates that the VI-based phenology metric was estimated too early, and negative values indicate the VI-based metric was estimated too late. Significant vegetation indices are highlighted in bold.

Vegetation index	SOS		SINK		POS		SOURCE		EOS	
	Mean	Std dev	Mean	Std dev	Mean	Std dev	Mean	Std dev	Mean	Std dev
Maize										
EVI	**4.27**	**14.14**	28.00	18.21	**−11.20**	**20.26**	**−6.40**	**14.01**	7.20	15.2956
GNDVI	−3.73	24.16	27.33	30.98	−11.84	23.22	−27.43	27.27	−13.71	28.365
LWSI	−23.20	17.87	−3.00	14.77	−13.76	23.72	−3.00	20.92	9.00	20.702
MSI	10.67	40.42	54.00	56.17	−1.92	61.68	58.67	132.29	72.00	128.7975
NDI7	−18.67	15.32	**6.00**	**18.41**	−13.76	23.72	−21.33	18.76	−8.89	21.3333
NDSVI	−8.53	36.97	10.67	41.12	−1.92	26.46	−2.18	21.79	10.91	19.6848
NDTI	−10.13	39.82	9.33	38.57	−11.20	36.66	−0.89	76.78	11.56	75.8009
NDVI	3.20	19.78	22.00	20.22	−12.48	24.12	−16.80	21.48	−3.20	24.2065
SAVI	10.67	14.40	33.33	17.34	**−10.24**	**20.72**	**−15.20**	**13.83**	−1.60	14.9904
STI	−30.40	9.66	**−6.00**	**17.44**	−15.36	26.42	−30.22	19.91	−16.00	23.6643
Soybean										
EVI	32.00	28.84	57.33	26.97	−1.23	19.55	−34.67	12.04	**−21.33**	**12.04**
GNDVI	5.33	32.33	38.67	23.96	−1.85	16.70	**−41.60**	**8.76**	−27.20	7.1554
LWSI	−52.00	5.66	**−11.20**	**9.12**	−10.46	18.00	−24.00	9.24	−16.00	9.2376
MSI	26.67	37.81	45.33	38.75	−0.62	16.80	−6.40	35.51	8.00	30.4631
NDI7	−13.33	46.88	14.67	41.54	**−10.46**	**18.00**	−33.33	12.82	−20.00	14.0855
NDSVI	**29.33**	**12.22**	50.67	15.73	−6.77	17.23	−41.33	35.93	−28.00	30.2523
NDTI	−12.00	50.91	0.00	38.09	29.54	79.09	44.00	121.09	57.33	117.512
NDVI	32.00	28.84	61.33	29.79	**−8.00**	**16.97**	−36.80	13.39	−22.40	11.8659
SAVI	32.00	28.84	57.33	26.97	**−8.00**	**17.28**	−36.00	12.13	−22.67	10.6333
STI	−8.00	44.54	2.67	37.07	−12.92	19.19	**−24.00**	**7.16**	**−10.67**	**10.9301**
Maize and soybean										
EVI	**8.89**	**19.38**	37.78	25.12	**−7.79**	**20.33**	−17.00	19.13	−3.50	19.81
GNDVI	−2.22	24.82	31.11	28.63	**−8.42**	**21.53**	−33.33	22.06	−19.33	22.49
LWSI	−28.00	19.74	**−6.15**	**13.13**	−12.63	21.74	−10.00	20.22	0.67	21.15
MSI	13.33	39.38	51.11	50.01	−1.47	50.59	29.09	102.03	42.91	98.91
NDI7	−17.78	21.35	8.89	27.29	**−12.63**	**21.74**	−26.13	17.23	**−13.33**	**19.04**
NDSVI	−2.22	36.79	24.00	39.29	−3.58	23.58	−16.00	32.74	−2.82	29.93
NDTI	−10.35	39.37	7.00	37.40	2.74	57.31	17.07	95.52	29.87	93.56
NDVI	**8.00**	**23.28**	35.11	29.82	−10.95	21.80	−23.47	21.05	−9.60	22.47
SAVI	14.22	18.32	41.33	23.32	**−9.47**	**19.41**	−23.00	16.49	**−9.50**	**16.84**
STI	−26.67	19.60	−3.11	24.87	−14.53	23.95	−27.73	15.96	**−13.87**	**19.23**

(29.33 days), and a significant t statistic. This indicates that NDSVI estimated the SOS 29 days too early. NDSVI was the only significant VI with an MSD less than 30 days and a standard deviation less than 20 days. The standard deviations of the signed differences were larger in soybean fields than in maize, partially as a result of the limited number of site years available.

The VI that best captured the day of carbon SINK in a maize field was the STI with an MSD of −6.00 days, a standard deviation of 17.44 days, and a significant t statistic. This indicates that the VI-based phenology using STI estimated the day of year when the field became a carbon SINK 6 days later, which is less than the 8-day time stamp between data points. Normalized difference index (NDI7) performed similarly by predicting the SINK point 6 days too early, with a standard deviation of 18.41 days.

Meanwhile, the significant VIs that best captured the day of carbon SINK in soybean fields were the land surface water index (LWSI) with an MSD of −11.20 days with a standard deviation of 9.12 days. No other VIs were able to adequately represent the SINK date in soybean fields.

In maize fields the NEE measurements had an average of 24 days difference between SOS and day of carbon SINK. This means there are three 8-day data points between SOS and day of carbon SINK in maize fields. This underscores how few data passages are available between these two metrics, and missing observations that occur in satellite remote sensing as a result of clouds may miss these transition points in CFP. The average 24-day bias was reflected in the differences from VI-based metrics because the same start of season

metric obtained from VI-based metrics were used to compare against NEE-based SOS and SINK dates.

In soybean fields the average difference between SOS and SINK dates as determined by NEE measurements were 8 days. This is significantly shorter than maize fields, and there is only one time stamp between SOS and SINK dates for maize. This means if there is one missing remote sensing scan that the SOS or SINK can be missed. This would indicate the need for finer-temporal-resolution datasets.

b. Peak of season

When estimating the time of peak productivity in maize, the VI that had a significant t statistic and the best fit was EVI, which had an MSD of -11.20 days and a standard deviation of 14.01 days. SAVI was also significant, and had an MSD of -10.24 days and a standard deviation of 20.72 days. The other eight VI MSDs were between $\sim$10 and 16 days late, which would indicate that the POS as determined from VI-based metrics was between 8 and 16 days late. The VIs with the most consistent performance were EVI and SAVI.

The VIs that identified POS in the carbon uptake in soybean fields from VI-based phenology metrics with a small MSD, a small standard deviation, and a significant t statistic were NDSVI, NDVI, and SAVI with a mean signed difference of -6.77, -8.00, and -8.00 days, respectively, and a standard deviation of 17.23, 16.97, and 17.28 days, respectively. All the VIs tested had very good agreement across sites with a standard deviation in the signed differences between 16 and 20 days; however, several VIs were deemed insignificant. There was a significantly tighter spread in the MSDs for soybean than maize. The best metric for identifying POS in soybean fields was NDSVI because it had the smallest MSD and a smaller standard deviation.

c. End of season and SOURCE

Estimating the time when the maize field became a carbon SOURCE had similar challenges as those found when estimating SOS and SINK. The MSDs were large across most VIs tested (see Table 3); however, they were the more consistent with a smaller standard deviation. The significant VI that best captured the day of carbon SOURCE for maize was EVI with an MSD of -6.40 days and a standard deviation of 14.01 days. SAVI was able to estimate NEE-based metrics from VI-based metrics consistently with a larger MSD. The VIs that performed best in estimating the day of carbon source were consistently 8–16 days late. There was a small mean signed difference (-0.89 days) for the normalized difference tillage index (NDTI), but this index was not selected as a good metric for the SOURCE date

because of the large standard deviation (76.89 days) and the t statistic deemed the VI to be insignificant.

The estimation of the SOURCE date from VI-based phenological metrics for soybean fields had a similar delay pattern to what was found in maize. The VIs that most effectively estimated the day of carbon SOURCE were LWSI and STI. Both VIs had a larger MSD of -24.00 days, but they had a standard deviation less than 10 days, which is within one 8-day time stamp.

The best VIs for estimating EOS dynamics in maize fields were EVI and SAVI, where both VIs had significant t statistics. The MSD for EVI was 7.20 days with a standard deviation of 15.29 days, and SAVI had an MSD of -1.60 days with a standard deviation of 14.99 days. This means that EVI and SAVI could accurately estimate NEE-based EOS within 0–8 days.

When estimating the EOS in soybean fields, all VIs had a higher value in MSD. On average the MSD ranged from 16 to 28 days between NEE-based and VI-based phenology metrics. The VI that had the smallest mean signed difference and standard deviation was the STI with an MSD of -10.67 days and a standard deviation of 10.93 days. Other alternatives for estimating the EOS from VI-based phenology in preference order were LWSI, the green normalized difference vegetation index (GNDVI), and EVI. The statistics for these additional three VIs can be found in Table 3.

d. Metric comparison for soybean and maize fields combined

The MSDs were computed for all phenology metrics where crop type was not considered. When crop type was not considered when estimating CFP metrics, there were higher standard deviations of the MSDs. As expected, the MSD was approximately the mean of the two MSDs of soybean and maize separately. A summary of these statistics is found in Table 3.

e. Total NEE during carbon uptake period

Accurately capturing the CFP is important for estimating the total carbon uptake that occurs from the day of carbon SINK to the day of carbon SOURCE. The total NEE was summed using $SINK_{NEE}$ and $SOURCE_{NEE}$ NEE-based phenology metrics, and was compared to the total NEE when using VI-based estimated SOS_{VI} and EOS_{VI} phenology metrics. The results found that the total NEE was less negative than ground-based results; the results for maize/soybean rotation (US-Ne2) can be seen in Fig. 5. In 2007 there were significant data gaps as a result of cloud cover, so the SOS and EOS could not be calculated for this year for this station. In this example the VI-based phenology metrics were not able to capture the true sum of NEE
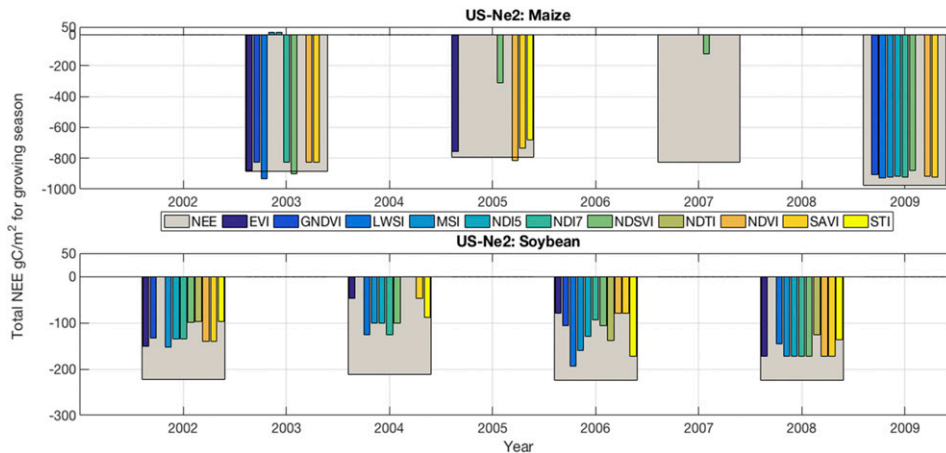
FIG. 5. Total NEE during the carbon uptake period, from day of carbon sink to day of carbon source, as computed from NEE-based phenology metrics is plotted (large gray bars) for soybean and maize at the US-Ne2 AmeriFlux site. Sum of NEE using the day of SOS and EOS as computed by the VI-based phenology metrics (colored bars). Some VI-based phenology metrics do not appear on the plot as a result of low sums in NEE. Occasionally VI-based phenology metrics were not able to be computed or resulted in values very close in days as a result of missing observations from cloud cover.

during the carbon uptake period and typically under-estimated the total carbon uptake for the year. The same pattern was observed in the other four sites in this analysis. The life cycle and structure of maize and soybean are starkly different, which results in different reflectance between each crop type; greater carbon uptake in maize compared to soybean affirms the need for crop type spatiotemporal models.

5. Discussion

a. Start of season and SINK date

SOS and SINK dates were best captured by indices other than those used in most literature, which are EVI and NDVI; these varying indices also varied by crop type. Balzarolo et al. (2016) assessed six indices, whereas we assessed four of the six in our analysis. We identified that EVI performed better than NDVI in croplands when identifying phenological metrics. Our results support that EVI and NDVI can accurately estimate SOS with biases of approximately eight days when crop type is not considered. More specifically, our results also show the MSDs are larger than 30 days when using EVI to estimate SOS for soybean, but it performs with acceptable biases of less than eight days for maize fields for SOS.

Contrary to Balzarolo et al. (2016), we found that NDSVI is a better metric for estimating SOS for soybean. The results presented here are consistent with Balzarolo et al. (2016) that EVI performs best in croplands for identifying CFP metrics, but that it is more accurate in maize fields (C_4 photosynthetic pathway) than soybean

fields (C_3 photosynthetic pathway). The biases tended to be larger for soybean crops than maize because of differences in early developmental stages and in the timing of the point of photosynthetic acclimation. Depending on the temperature and moisture availability, the plant-to-emergence time for soybeans is 5–21 days and for maize 7–10 days. The period from vegetation emergence to peak photosynthetic uptake [which typically occurs in reproductive phases 1–2 (R1–R2)] is 39–71 days in soybeans and 69–75 days in maize. Soybean goes through 6 growing stages, while maize goes through 18 growing phases before beginning the reproductive phase (Fehr et al. 1971; Licht 2014; Abendroth et al. 2011). This apparent temporal mismatch is a strong contributor to why different VIs perform better for soybean than maize. Previous work by Klosterman et al. (2014) is consistent with our findings because they found there was a 2–8-day lag in phenology metrics derived from satellite remote sensing compared to those derived from PhenoCams.

The LWSI is the best VI for soybean when estimating the day of year when the crop field became a carbon SINK. This index relies on the use of the NIR and SWIR2 reflectance bands, which are sensitive to the amount of water (SWIR2), and there is a higher amount of reflectance of NIR from chloroplasts, which contain chlorophyll (Jensen 2005). However, maize was most sensitive to EVI and SAVI, which rely on the red and NIR bands. Water reflects a majority of the NIR and SWIR2 wavelengths (Jensen 2005). Both maize and soybean are highly sensitive to water availability and temperature in stages of growth (Fehr et al. 1971;
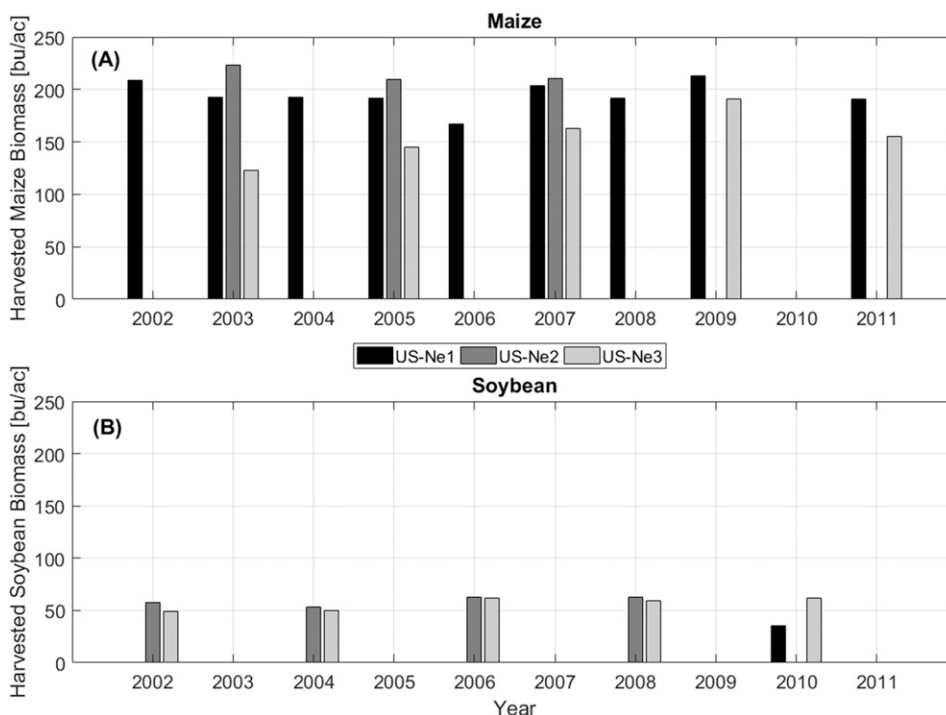
FIG. 6. Total harvested biomass for (a) maize and (b) soybean for the three stations located in Nebraska (US-Ne1, US-Ne2, US-Ne3). Harvested biomass is significantly higher for maize than soybean annually.

Abendroth et al. 2011), making it logical that both crops make use of a VI that includes bands that are sensitive to water. However, maize relied on VIs that made use of the red band. The red band is where a large amount light is absorbed by the mesophyll as a result of chlorophyll content, making it the best band for chlorophyll absorption characteristics. In the SWIR2 and NIR bands, there is scattering of these wavelengths in the spongy mesophyll (Jensen 2005). This is consistent with the findings of Viña et al. (2011), who found the red band to be more significant for maize in the early part of the growing season than soybean. This occurs because there is significantly more scattering of longer wavelengths in soybean leaves, which results in much higher reflectance in soybeans compared to maize (Viña et al. 2011).

b. Peak of season

We found POS the easiest transition point to identify remotely. The metrics for soybean had a smaller standard deviation and smaller MSDs than maize metrics, indicating that soybean POS can be estimated with better certainty than maize. Maize has a peak in carbon uptake approximately 8–16 days after the peak greenness, while the peak in greenness is approximately the same as the peak in carbon uptake in soybean fields. This may be due to the larger amount of biomass that is visible when viewing maize fields; this was confirmed with the

biomass data available for US-Ne* stations from AmeriFlux (Fig. 6). This means there is a greater leaf area index (LAI). High LAI can saturate the reflectance in a pixel, and there may be points in the time series where the satellite is unable to detect changes in greenness.

Reflectance saturation is the cause of the 10-day bias in several of the VIs for maize when using SAVI or EVI. Maize transitions to a new vegetation stage every 2 days, and so the 8-day temporal resolution may be too coarse to capture changes in maize greenness. This may result in the sensor missing the appropriate scan time for maximum carbon uptake, which occurs in reproductive phases 1–2 (Abendroth et al. 2011). It is vitally important to capture the peak LAI in maize because the maximum LAI is linked to maximum daytime NEE and gross primary production (Suyker et al. 2004). Meanwhile, soybean has a smaller LAI and therefore will not saturate the remote sensing pixel; as a result the POS is easier to capture.

While POS is easiest to identify, the most effective metrics are EVI and SAVI for maize fields and NDSVI, NDVI, and SAVI for soybean fields. All of these VIs make use of the red reflectance band and the secondary bands are NIR and SWIR1, respectively. The results agree well with the findings in Viña et al. (2011), who found that soybean had an increasing reflectance with increasing wavelength, while maize had a lower reflectance in longer wavelengths when compared to soybean,

indicating that soybean and maize needed different remote sensing algorithms for estimating LAI, and therefore VI-based CFP metrics.

c. End of season and SOURCE date

EOS and SOURCE dates were very difficult to estimate, but this is not exclusive to agricultural crops. Klosterman et al. (2014) reported larger root-mean-square differences between all phenology metrics derived from satellite remote sensing and PhenoCams. This is caused by complicated relationships between senescence and carbon fluxes as a result of foliar pigments, meteorological conditions, and environmental stresses, which will affect all plants (Garrity et al. 2011). The differences in structural leaf orientation and chlorophyll content between soybean and maize leaves will cause these crops to appear differently during senescence (Viña et al. 2011). In maize fields, EOS and SOURCE dates had higher standard deviation than those found in soybean fields. In both cases the MSDs were high but consistent. For instance, there was a three 8-day time stamp bias (24 days) between the EOS estimated by VI-based phenology and the NEE-based day of carbon SOURCE; this bias will be used to estimate the day of SOURCE in future work.

d. Implications and future work

One limitation of the method demonstrated here was that the CFP metrics could not be estimated in maize and soybean fields that had two crop rotations within the same year. This resulted in two growing seasons, making the differentiation programmatically challenging. The years where maize and soybean were grown at the US-ARM station also had wheat grown earlier in the year. As a result of this challenge, the US-ARM station was omitted from the MSDs. Crop fields where there are two crop rotations per year will not perform well in this methodology, unless the dates are known when each crop occurred during the year.

Viña et al. (2011) determined that the differences in the reflectance of soybean and maize leaves at different wavelengths during peak LAI were due to differences in leaf structure and leaf chlorophyll content. Despite soybeans having a smaller LAI, soybean had higher reflectance than maize in longer wavelengths as a result of higher chlorophyll content in the adaxial side of soybean leaves and lower water content. In maize leaves, there is a larger depth of light penetration. Since the chlorophyll content is constant throughout the maize leaves, deeper light penetration leads to more light absorption in the shorter wavelengths. Meanwhile, because the chlorophyll content varies between the adaxial and abaxial sides of soybean leaves, the light penetration

reaches only the spongy layer, which has lower chlorophyll content and results in less light absorption.

The results of this analysis show that the differences between reflectance and physiological composition between maize and soybean means each crop will appear different in remote sensing datasets. The downscaling process amplifies these differences. One limitation of using downscaled MODIS imagery is that if a clear-sky and snow-free remote sensing pair of Landsat and MODIS cannot be identified before the true SOS and/or after EOS, then the full growing season cannot be observed. In this case VI-based phenology metrics will be missing or incorrect. This is especially true in humid environments, where cloud cover is more frequent, and in northern latitudes, where snow is prevalent for long periods, making Landsat's 16-day revisit time insufficient. If missing pairs occur within the growing season, then incorrect VI-based phenology metrics will result regardless of the VI used. A different downscaling algorithm that does not require Landsat imagery would be required to address this limitation.

As discussed above, it is common to model either NEE, gross primary production, or NEP with one agricultural subgroup. This work shows that using the correct VI for an individual field could improve model results. Future work will need to make use of land-cover datasets, such as the USDA's cropland data layer, so that this analysis can be expanded outside of preidentified cropland fields and that the impacts of maize and soybean agriculture on carbon exchanges in the United States can be identified.

This approach, however, does have a limitation. When using 8-day temporal resolution datasets, a single missing remote sensing image can cause a true phenology metric to be missed. This will cause total NEE values to be too high, as demonstrated in Fig. 5. Future work may have to consider using daily MODIS imagery to limit the number of holes that may occur as a result of clouds and snow cover, and to capture changes in the vegetation that are occurring at time scales smaller than 8 days (especially during the vegetative stage).

6. Conclusions

Modeling and mapping CFP in agricultural systems require different strategies based on crop type when using VI-based products. Here we show that a single VI cannot accurately capture the full CFP for all crops because of the differences in crop life cycle and crop physiology. This work is important because incorrect CFP metrics can cause modeled NEE to be overestimate or underestimated. Therefore, in future work an empirical model will be developed and tested to estimate

carbon uptake period from VI-based indices that is crop type dependent, beginning with maize and soybean crops. This will help to give a better understanding of which reflectance bands best capture carbon dynamics in maize and soybean fields. A better estimation of carbon flux dynamics will help to provide better information about the regional impact of growing maize and soybean in the U.S. Great Plains on carbon flux dynamics, which will inform future climate models as the cultivation of maize and soybean expands across the United States.

REFERENCES

Abendroth, L. J., R. W. Elmore, M. J. Boyer, and S. K. Marlay, 2011: Corn growth and development. Iowa State University Extension and Outreach PMR 1009, 50 pp., https://store.extension.iastate.edu/Product/Corn-Growth-and-Development.

Baldocchi, D., and Coauthors, 2001: FLUXNET: A new tool to study the temporal and spatial variability of ecosystem-scale carbon dioxide, water vapor, and energy flux densities. *Bull. Amer. Meteor. Soc.*, **82**, 2415–2434, https://doi.org/10.1175/1520-0477(2001)082<2415:FANTTS>2.3.CO;2.

Balzarolo, M., and Coauthors, 2016: Matching the phenology of Net Ecosystem Exchange and vegetation indices estimated with MODIS and FLUXNET in-situ observations. *Remote Sens. Environ.*, **174**, 290–300, https://doi.org/10.1016/j.rse.2015.12.017.

Bonan, G., 2008: *Ecological Climatology: Concepts and Applications.* 2nd ed. Cambridge University Press, 278 pp.

Cicuéndez, V., and Coauthors, 2015: Assessment of soil respiration patterns in an irrigated corn field based on spectral information acquired by field spectroscopy. *Agric. Ecosyst. Environ.*, **212**, 158–167, https://doi.org/10.1016/j.agee.2015.06.020.

DeMers, M. N., 2002: *GIS Modeling in Raster.* John Wiley & Sons, Inc., 203 pp.

Dong, J., and Coauthors, 2015: Comparison of four EVI-based models for estimating gross primary production of maize and soybean croplands and tallgrass prairie under severe drought. *Remote Sens. Environ.*, **162**, 154–168, https://doi.org/10.1016/j.rse.2015.02.022.

Fang, B., V. Lakshmi, R. Bindlish, T. J. Jackson, M. Cosh, and J. Basara, 2013: Passive microwave soil moisture downscaling using vegetation index and skin surface temperature. *Vadose Zone J.*, **12**, https://doi.org/10.2136/vzj2013.05.0089.

Fehr, W. R., C. E. Caviness, D. T. Burmood, and J. S. Pennington, 1971: Stage of development descriptions for soybeans, Glycine max (L.) Merrill. *Crop Sci.*, **11**, 929–931, https://doi.org/10.2135/cropsci1971.0011183X001100060051x.

Frank, A. B., and W. A. Dugas, 2001: Carbon dioxide fluxes over a northern, semiarid, mixed-grass prairie. *Agric. For. Meteor.*, **108**, 317–326, https://doi.org/10.1016/S0168-1923(01)00238-6.

——, and J. F. Karn, 2003: Vegetation indices, CO_2 flux, and biomass for northern plains grasslands. *J. Range Manage.*, **56**, 382–387, https://doi.org/10.2307/4004043.

Fu, D., and Coauthors, 2014: Estimating landscape net ecosystem exchange at high spatial–temporal resolution based on Landsat data, an improved upscaling model framework, and eddy covariance flux measurements. *Remote Sens. Environ.*, **141**, 90–104, https://doi.org/10.1016/j.rse.2013.10.029.

Gao, F., J. Masek, M. Schwaller, and F. Hall, 2006: On the blending of the Landsat and MODIS surface reflectance: Predicting daily Landsat surface reflectance. *IEEE Trans. Geosci. Remote Sens.*, **44**, 2207–2218, https://doi.org/10.1109/TGRS.2006.872081.

Garrity, S. R., G. Bohrer, K. D. Maurer, K. L. Mueller, C. S. Vogel, and P. S. Curtis, 2011: A comparison of multiple phenology data sources for estimating seasonal transitions in deciduous forest carbon exchange. *Agric. For. Meteor.*, **151**, 1741–1752, https://doi.org/10.1016/j.agrformet.2011.07.008.

Gebremedhin, M. T., H. W. Loescher, and T. D. Tsegaye, 2012: Carbon balance of no-till soybean with winter wheat cover crop in the southeastern United States. *Agron. J.*, **104**, 1321, https://doi.org/10.2134/agronj2012.0072.

Gitelson, A. A., and M. N. Merzlyak, 1998: Remote sensing of chlorophyll concentration in higher plant leaves. *Adv. Space Res.*, **22**, 689–692, https://doi.org/10.1016/S0273-1177(97)01133-2.

Griffis, T. J., and Coauthors, 2011: Oxygen isotope composition of evapotranspiration and its relation to C_4 photosynthetic discrimination. *J. Geophys. Res.*, **116**, G01035, https://doi.org/10.1029/2010JG001514.

Guo, X., K. P. Price, and J. M. Stiles, 2003: Grasslands discriminant analysis using Landsat TM single and multitemporal data. *Photogramm. Eng. Remote Sens.*, **11**, 1255–1262, https://doi.org/10.14358/pers.69.11.1255.

Horst, T. W., and J. C. Weil, 1994: How far is far enough?: The fetch requirements for micrometeorological measurement of surface fluxes. *J. Atmos. Oceanic Technol.*, **11**, 1018–1025, https://doi.org/10.1175/1520-0426(1994)011<1018:HFIFET>2.0.CO;2.

Huete, A. R., 1988: A soil-adjusted vegetation index (SAVI). *Remote Sens. Environ.*, **25**, 295–309, https://doi.org/10.1016/0034-4257(88)90106-X.

——, C. Justice, and H. Liu, 1994: Development of vegetation and soil indices for MODIS-EOS. *Remote Sens. Environ.*, **49**, 224–234, https://doi.org/10.1016/0034-4257(94)90018-3.

——, H. Q. Liu, K. Batchily, and W. van Leeuwen, 1997: A comparison of vegetation indices over a global set of TM images for EOS-MODIS. *Remote Sens. Environ.*, **59**, 440–451, https://doi.org/10.1016/S0034-4257(96)00112-5.

——, K. Didan, T. Miura, E. P. Rodriguez, X. Gao, and L. G. Ferreira, 2002: Overview of the radiometric and biophysical performance of the MODIS vegetation indices. *Remote Sens. Environ.*, **83**, 195–213, https://doi.org/10.1016/S0034-4257(02)00096-2.

Jensen, J. R., 2005: *Introductory Digital Image Processing: A Remote Sensing Perspective*. 3rd ed. Prentice Hall Series on Geographic Information Science, Prentice Hall, 526 pp.

Kljun, N., P. Calanca, M. W. Rotach, and H. P. Schmid, 2015: A simple two-dimensional parameterisation for Flux Footprint Prediction (FFP). *Geosci. Model Dev.*, **8**, 3695–3713, https://doi.org/10.5194/gmd-8-3695-2015.

Klosterman, S. T., and Coauthors, 2014: Evaluating remote sensing of deciduous forest phenology at multiple spatial scales using PhenoCam imagery. *Biogeosciences*, **11**, 4305–4320, https://doi.org/10.5194/bg-11-4305-2014.

Leclerc, M. Y., and T. Foken, 2014: *Footprints in Micrometeorology and Ecology*. Springer-Verlag, 239 pp., https://doi.org/10.1007/978-3-642-54545-0.

Le Quéré, C., and Coauthors, 2015: Global carbon budget 2015. *Earth Syst. Sci. Data*, **7**, 349–396, https://doi.org/10.5194/essd-7-349-2015.

Licht, M., 2014: Soybean growth and development. Iowa State University Extension and Outreach PM 1945, 28 pp., https://store.extension.iastate.edu/Product/6451.

Masek, J. G., and Coauthors, 2006: A Landsat surface reflectance dataset for North America, 1990–2000. *IEEE Geosci. Remote Sens. Lett.*, **3**, 68–72, https://doi.org/10.1109/LGRS.2005.857030.

McNairn, H., and R. Protz, 1993: Mapping corn residue cover on agricultural fields in Oxford County, Ontario, using Thematic Mapper. *Can. J. Remote Sens.*, **19**, 152–159, https://doi.org/10.1080/07038992.1993.10874543.

Noormets, A., J. Chen, L. Gu, and A. Desai, 2009: The phenology of gross ecosystem productivity and ecosystem respiration in temperate hardwood and conifer chronosequences. *Phenology of Ecosystem Processes: Applications in Global Change Research*, A. Noormets, Ed., Springer, 59–85.

Papale, D., and Coauthors, 2015: Effect of spatial sampling from European flux towers for estimating carbon and water fluxes with artificial neural networks. *J. Geophys Res. Biogeosci.*, **120**, 1941–1957, https://doi.org/10.1002/2015JG002997.

Peng, D., and Coauthors, 2017: Intercomparison and evaluation of spring phenology products using National Phenology Network and AmeriFlux observations in the contiguous United States. *Agric. For. Meteor.*, **242**, 33–46, https://doi.org/10.1016/j.agrformet.2017.04.009.

Price, K. P., X. Guo, and J. M. Stiles, 2002: Optimal Landsat TM band combinations and vegetation indices for discrimination of six grassland types in eastern Kansas. *Int. J. Remote Sens.*, **23**, 5031–5042, https://doi.org/10.1080/01431160210121764.

Qi, J., R. Marsett, P. Heilman, S. Bieden-Bender, S. Moran, D. Goodrich, and M. Weltz, 2002: RANGES improves satellite-based information and land cover assessments in southwest United States. *Eos, Trans. Amer. Geophys. Union*, **83**, 601–606, https://doi.org/10.1029/2002EO000411.

Raz-Yaseef, N., D. Billesbach, M. L. Fischer, S. C. Biraud, S. A. Gunter, J. A. Bradford, and M. S. Torn, 2015: Vulnerability of crops and native grasses to summer drying in the U.S. Southern Great Plains. *Agric. Ecosyst. Environ.*, **213**, 209–218, https://doi.org/10.1016/j.agee.2015.07.021.

Rock, B. N., J. E. Vogelmann, D. L. Williams, A. F. Vogelmann, and T. Hoshizaki, 1986: Remote detection of forest damage: Plant responses to stress may have spectral ''signatures'' that could be used to map, monitor, and measure forest damage. *Bioscience*, **36**, 439–445, https://doi.org/10.2307/1310339.

Rouse, J. W., Jr., R. H. Haas, J. A. Schell, and D. W. Deering, 1974: Monitoring vegetation systems in the Great Plains with ERTS. Third Earth Resources Technology Satellite-1 Symposium: Volume 1; Technical presentations, section B, S. C. Freden, E. P. Mercanti, and M. A. Becker, Eds., NASA Special Publ. NASA-SP-351-VOL-1-SECT-B, A 20, 309–317.

Running, S. W., D. D. Baldocchi, D. P. Turner, S. T. Gower, P. S. Bakwin, and K. A. Hibbard, 1999: A global terrestrial monitoring network integrating tower fluxes, flask sampling, ecosystem modeling and EOS satellite data. *Remote Sens. Environ.*, **70**, 108–127, https://doi.org/10.1016/S0034-4257(99)00061-9.

Shen, Y., and C. B. Tanner, 1990: Radiative and conductive transport of heat through flail chopped corn residue. *Soil Sci. Soc. Amer. J.*, **54**, 633–658, https://doi.org/10.2136/sssaj1990.03615995005400030005x.

Suyker, A., S. Verma, G. Burba, T. Arkebauer, D. Walters, and K. Hubbard, 2004: Growing season carbon dioxide exchange in irrigated and rainfed maize. *Agric. For. Meteor.*, **124**, 1–13, https://doi.org/10.1016/j.agrformet.2004.01.011.

van Deventeer, A. P., A. D. Ward, P. H. Gowda, and J. G. Lyon, 1997: Using Thematic Mapper data to identify contrasting soil plains and tillage practices. *Photogramm. Eng. Remote Sens.*, **63**, 87–93.

Verma, S. B., and Coauthors, 2005: Annual carbon dioxide exchange in irrigated and rainfed maize-based agroecosystems. *Agric. For. Meteor.*, **131**, 77–96, https://doi.org/10.1016/j.agrformet.2005.05.003.

Vermote, E., 2015: MOD09A1 MODIS/Terra Surface Reflectance 8-Day L3 Global 500m SIN Grid V006. NASA EOSDIS Land Processes Distributed Active Archive Center, accessed 15 June 2015, http://doi.org/10.5067/MODIS/MOD09A1.006.

Viña, A., A. A. Gitelson, A. L. Nguy-Robertson, and Y. Peng, 2011: Comparison of different vegetation indices for the remote assessment of green leaf area index of crops. *Remote Sens. Environ.*, **115**, 3468–3478, https://doi.org/10.1016/j.rse.2011.08.010.

Vose, R. S., and Coauthors, 2014: NOAA's Gridded Climate Divisional Dataset (CLIMDIV). Subset used: Local Climatological Dataset. NOAA National Climatic Data Center, accessed 16 January 2017, https://doi.org/10.7289/V5M32STR.

Vuichard, N., and D. Papale, 2015: Filling the gaps in meteorological continuous data measured at FLUXNET sites with ERA-Interim reanalysis. *Earth Syst. Sci. Data*, **7**, 157–171, https://doi.org/10.5194/essd-7-157-2015.

Walker, J. J., K. M. de Beurs, R. H. Wynne, and F. Gao, 2012: Evaluation of Landsat and MODIS data fusion products for analysis of dryland forest phenology. *Remote Sens. Environ.*, **117**, 381–393, https://doi.org/10.1016/j.rse.2011.10.014.

Wan, Z., S. Hook, and G. Hulley, 2015: MOD11A2 MODIS/Terra Land Surface Temperature/Emissivity 8-Day L3 Global 1 km SIN Grid V006. NASA EODIS Land Processes Distributed Active Archive Center, accessed 16 June 2015, https://doi.org/10.5067/MODIS/MOD11A2.006.

Wang, C., F. B. Fritschi, G. Stacey, and Z. Yang, 2011: Phenology-based assessment of perennial energy crops in North American tallgrass prairie. *Ann. Assoc. Amer. Geogr.*, **101**, 742–751, https://doi.org/10.1080/00045608.2011.567934.

——, E. R. Hunt Jr., L. Zhang, and H. Guo, 2013: Phenology-assisted classification of C3 and C4 grasses in the U.S. Great

Plains and their climate dependency with MODIS time series. *Remote Sens. Environ.*, **138**, 90–101, https://doi.org/10.1016/j.rse.2013.07.025.

Wu, C., and Coauthors, 2012: Interannual and spatial impacts of phenological transitions, growing season length, and spring and autumn temperatures on carbon sequestration: A North America flux data synthesis. *Global Planet. Change*, **92–93**, 179–190, https://doi.org/10.1016/j.gloplacha.2012.05.021.

——, and Coauthors, 2017: Land surface phenology derived from normalized difference vegetation index (NDVI) at global FLUXNET sites. *Agric. For. Meteor.*, **233**, 171–182, https://doi.org/10.1016/j.agrformet.2016.11.193.

Xiao, J., and Coauthors, 2011: Assessing net ecosystem carbon exchange of U.S. terrestrial ecosystems by integrating eddy covariance flux measurements and satellite observations. *Agric. For. Meteor.*, **151**, 60–69, https://doi.org/10.1016/j.agrformet.2010.09.002.

Xiao, X., D. Hollinger, J. Aber, M. Goltz, E. A. Davidson, Q. Zhang, and B. Moore, 2004: Satellite-based modeling of gross primary production in an evergreen needleleaf forest. *Remote Sens. Environ.*, **89**, 519–534, https://doi.org/10.1016/j.rse.2003.11.008.

——, Q. Zhang, D. Hollinger, J. Aber, and B. Moore III, 2005: Modeling gross primary production of an evergreen needleleaf forest using MODIS and climate data. *Ecol. Appl.*, **15**, 954–969, https://doi.org/10.1890/04-0470.

Zhang, X., M. A. Friedl, C. B. Schaaf, A. H. Strahler, J. C. F. Hodges, F. Gao, B. C. Reed, and A. Huete, 2003: Monitoring vegetation phenology using MODIS. *Remote Sens. Environ.*, **84**, 471–475, https://doi.org/10.1016/S0034-4257(02)00135-9.

Zhu, X., J. Chen, F. Gao, X. Chen, and J. G. Masek, 2010: An enhanced spatial and temporal adaptive reflectance fusion model for complex heterogeneous regions. *Remote Sens. Environ.*, **114**, 2610–2623, https://doi.org/10.1016/j.rse.2010.05.032.